

A generalized approach to photon avalanche upconversion in luminescent nanocrystals

Artiom Skripka^{1,2*}, Minji Lee^{1,3}, Xiao Qi¹, Jia-Ahn Pan¹, Haoran Yang^{1,#}, Changhwan Lee⁴, P. James Schuck⁴, Bruce E. Cohen^{1,5}, Daniel Jaque^{2*} and Emory M. Chan^{1*}

¹The Molecular Foundry, Lawrence Berkeley National Laboratory, Berkeley, California 94720, United States

²Nanomaterials for Bioimaging Group, Departamento de Física de Materiales, Facultad de Ciencias, Universidad Autónoma de Madrid, Madrid, 28049, Spain

³Department of Chemical and Biomolecular Engineering, University of California Berkeley, Berkeley, California 94720, United States

⁴Department of Mechanical Engineering, Columbia University, New York, New York 10027, United States

⁵Division of Molecular Biophysics & Integrated Bioimaging, Lawrence Berkeley National Laboratory, Berkeley, California 94720, United States

#Present address: STMicroelectronics, Santa Clara, California, United States

*Corresponding authors: a_skripka@lbl.gov, daniel.jaque@uam.es, emchan@lbl.gov

Keywords: Upconversion, Photon Avalanche, Spectral Tuning, Nonlinear Emitters

Abstract: Photon avalanching nanoparticles (ANPs) exhibit extremely nonlinear upconverted emission valuable for sub-diffraction imaging, nanoscale sensing, and optical computing. Avalanching has been demonstrated with Tm³⁺, Nd³⁺ or Pr³⁺-doped nanocrystals, but their emission is limited to 600 and 800 nm, restricting applications. Here, we utilize Gd³⁺-assisted energy migration to tune the emission wavelengths of Tm³⁺-sensitized ANPs and generate highly nonlinear emission of Eu³⁺, Tb³⁺, Ho³⁺, and Er³⁺ ions. The upconversion intensities of these spectrally discrete ANPs scale with the nonlinearity factor $s = 10^{-17}$ under 1064 nm excitation at power densities as low as 6 kW·cm⁻². This strategy for imprinting avalanche behavior on remote emitters can be extended to fluorophores adjacent to ANPs, as we demonstrate with CdS/CdSe/CdS core/shell/shell quantum dots. ANPs with rationally designed energy transfer networks provide the means to transform conventional linear emitters into a highly nonlinear ones, expanding the use of photon avalanching in biological, chemical, and photonic applications.

Photon avalanching (PA) nanoparticles exhibit giant optical nonlinearities in their upconverted emission, such that a 10-20% increase in near infrared (NIR) excitation power can result in a 100- to 1000-fold increase in the emission intensity.^[1] PA behavior has been recently reported at room temperature in lanthanide (Ln^{3+})-doped nanocrystals of $\text{NaYF}_4:\text{Tm}^{3+}$,^[2] $\text{LiYF}_4:\text{Tm}^{3+}$, $\text{KPb}_2\text{Cl}_5:\text{Nd}^{3+}$, and $\text{NaYF}_4:\text{Yb}^{3+}, \text{Pr}^{3+}$.^[3-5] Their highly nonlinear responses, equivalent in some cases to those of >30-photon processes, has been utilized for nanoscale thermometers, molecular rulers, and most saliently, in sub-diffraction microscopy^[6-10] to achieve optical resolutions finer than 100 nm using conventional laser scanning microscope.^[2] However, these early avalanching nanoparticles (ANPs) mostly emit in the NIR (i.e., 800 nm), which limits the ability to probe multiple species independently at different visible wavelengths. To realize multiplexed applications of PA in imaging, sensing, and computing, ANPs with a broader wavelength range and more spectrally distinct luminescence profiles must be developed.

To diversify the library of ANPs using the few proven PA compositions, we utilized energy migration to transfer the nonlinear behavior of the Ln^{3+} ions responsible for avalanching to physically segregated emitters within the same nanocrystals and also to neighboring nanoparticles. Similar energy migration upconversion (EMU) approaches have been used in conventional upconverting nanoparticles (UCNPs) to tune upconversion with various Ln^{3+} emitters without changing underlying light sensitization mechanisms.^[11] Such physical decoupling is even more essential for ANPs, since the energy looping mechanism underpinning PA is particularly susceptible to quenching via cross-relaxation when additional ions are co-doped with avalanching ions. In ANPs, energy migration through Yb^{3+} ions was recently used to transfer the avalanching behavior of the $\text{Yb}^{3+}/\text{Pr}^{3+}$ PA system to ions that emit at visible wavelengths.^[5] This approach, however requires high excitation powers ($>70 \text{ kW}\cdot\text{cm}^{-2}$) and deconvolution of overlapping emission signals.

Here, we demonstrate how PA originating from Tm^{3+} ions can be harnessed together with EMU through Gd^{3+} ions to create a library of spectrally discrete ANPs with low avalanching thresholds and highly nonlinear emissions (**Figure 1**). We posited that reducing the number of avalanching Tm^{3+} ions (< 500) in small NaGdF_4 core nanoparticles ($< 7 \text{ nm}$) would accelerate saturation of the $^3\text{H}_4$ state and facilitate population of higher-energy levels of Tm^{3+} ($^1\text{D}_2$ and $^1\text{I}_6$).^[8,12] Subsequently, energy from these excited Tm^{3+} ions can be transferred to Gd^{3+} ions in the host matrix and relayed to any activator lanthanide ion (A^{3+}) in a nanocrystal. Because the energy of Gd^{3+} ions ($^6\text{P}_J$) is transferred from Tm^{3+} ions excited by multiple stages of PA, the high nonlinearity of PA can be preserved in the emission of A^{3+} ions (**Figure 1b**). Furthermore, EMU in ANPs can be extended to semiconductor quantum dots (QD), prompting highly nonlinear emission from an

ANP+QD avalanching complexes. Such avalanching complexes could enable development of long-range energy transfer sensors with high localization precision.^[9] Overall, the combination of Tm^{3+} -PA and Gd^{3+} -EMU provides a way to easily customize upconversion emission of ANPs, and the demonstrated spectrally discrete ANPs and avalanching complex enrich the palette of available nonlinear emitters for a range of photonic applications.

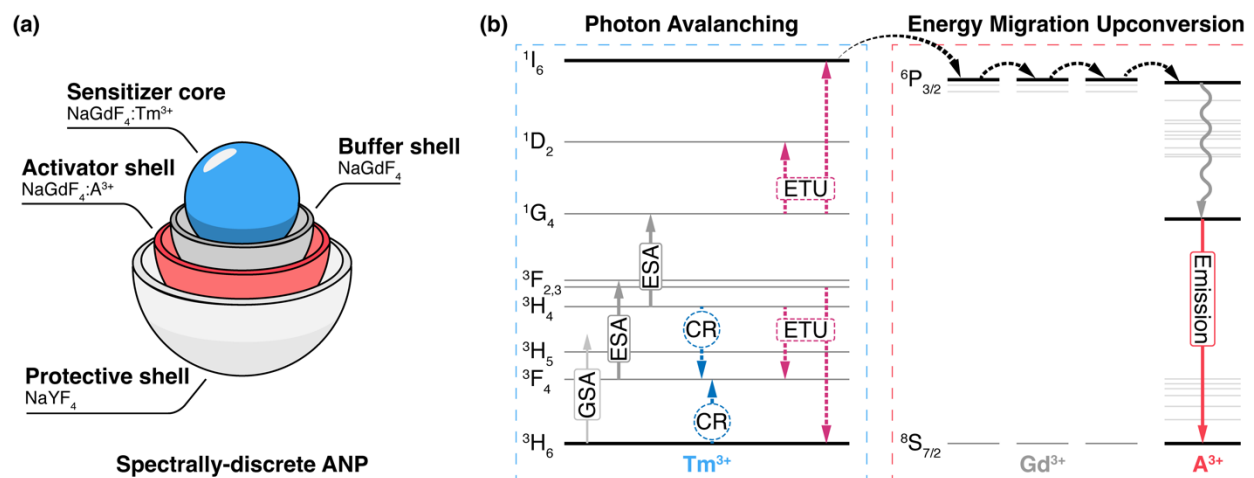


Figure 1. (a) Schematic representation of spectrally discrete ANPs consisting of the sensitizer core ($\text{NaGdF}_4:\text{Tm}^{3+}$), buffer shell (NaGdF_4), activator shell ($\text{NaGdF}_4:\text{A}^{3+}$), and the protective shell (NaYF_4). (b) Simplified energy level scheme and operation of spectrally discrete ANPs depicting 1064-nm-excited photon avalanche (GSA/ESA – ground/excited state absorption, CR – cross-relaxation, ETU – energy transfer upconversion), energy migration via Gd^{3+} ions, and instigation of visible avalanche upconversion in A^{3+} ions. Solid arrows – photon emission/absorption, dashed arrows – non-radiative energy transfer, wavy arrow – non-radiative multiphonon relaxation.

To implement this EMU photon avalanching architecture, we synthesized heterostructured ANPs consisting of a NaGdF_4 : 20 mol% Tm^{3+} sensitizer core, an undoped NaGdF_4 buffer shell, a NaGdF_4 : 15 mol% Eu^{3+} activator shell, and an undoped NaYF_4 outer shell (**Figure 2a, b**). Each shell of ANPs was grown sequentially by thermal decomposition of precursors using a nanoparticle synthesis robot (WANDA, see **Supporting Information S1** for details).^[13,14] An intermediate NaGdF_4 buffer shell was introduced to minimize direct energy transfer between sensitizer (Tm^{3+}) and activator (Eu^{3+}) ions, which could lead to quenching.^[15] Meanwhile, the protective NaYF_4 outer shell (**Figure S1** shows elemental mapping of Gd and Y) was used to reduce surface quenching and prevent excitation energy spill-out from the Gd^{3+} network.^[16] As synthesized, the Eu^{3+} -activated ANPs were observed to be pure $\text{Na}(\text{Y}/\text{Gd})\text{F}_4$ β -phase (**Figure**

S2) and less than 25 nm in diameter, determined by powder X-ray diffraction (XRD) and transmission electron microscopy (TEM), respectively. High crystallinity, small-size, and narrow size distribution (< 5%) ideally positions these ANPs for biological or nanoscale patterning applications.^[17–19]

Under 1064 nm irradiation the Eu³⁺-activated ANPs emitted 800 nm light characteristic of ³H₄ → ³H₆ radiative relaxation in avalanching Tm³⁺ ions (**Figure S3**).^[2,13] Interestingly, we observed a series of visible emission peaks at 510, 535, 555, 580, 590, and 615 nm, consistent with Eu³⁺ radiative transitions from ⁵D_J excited states (**Figure 2c**). The presence of Eu³⁺ emission confirms that energy migration from the Tm³⁺-doped core to the Eu³⁺-doped shell occurs through the Gd³⁺ sublattice, especially since no emission was detected with Tm³⁺-free core/shell NaGdF₄: 15 mol% Eu³⁺/NaYF₄ control nanoparticles excited at 1064 nm (**Supporting Information S3**). We note that the emission profile of Eu³⁺ in the 500-640 nm range has no overlap with Tm³⁺ upconversion and can be readily detected without the need for spectral deconvolution.

To determine whether PA occurs in these Eu³⁺-activated ANPs, we investigated the power dependence of the visible Eu³⁺ emission. With pump power (*P*) increasing above the 25 kW·cm⁻² threshold, the intensity (*I*) of the Eu³⁺ (⁵D₀ → ⁷F₂) line at 615 nm increased with the nonlinearity factor *s* = 14.6, where *s* is the slope of the log-log plot in **Figure 2d**, and *I* ∝ *P*^{*s*}. This steep power scaling of Eu³⁺ emission (i.e., *s* > 10) strongly suggests that the nonlinear behavior of the avalanching Tm³⁺ core is preserved in high energy states (e.g. ¹I₆) and can be transferred to Eu³⁺ ions by Gd³⁺-facilitated energy migration. As an additional indication of PA in Eu³⁺-activated ANPs, we observed prolonged rise times in time resolved luminescence of Eu³⁺ emission and their subsequent shortening with the increasing pump power (**Figure S4**), both of which are signatures of PA.^[1]

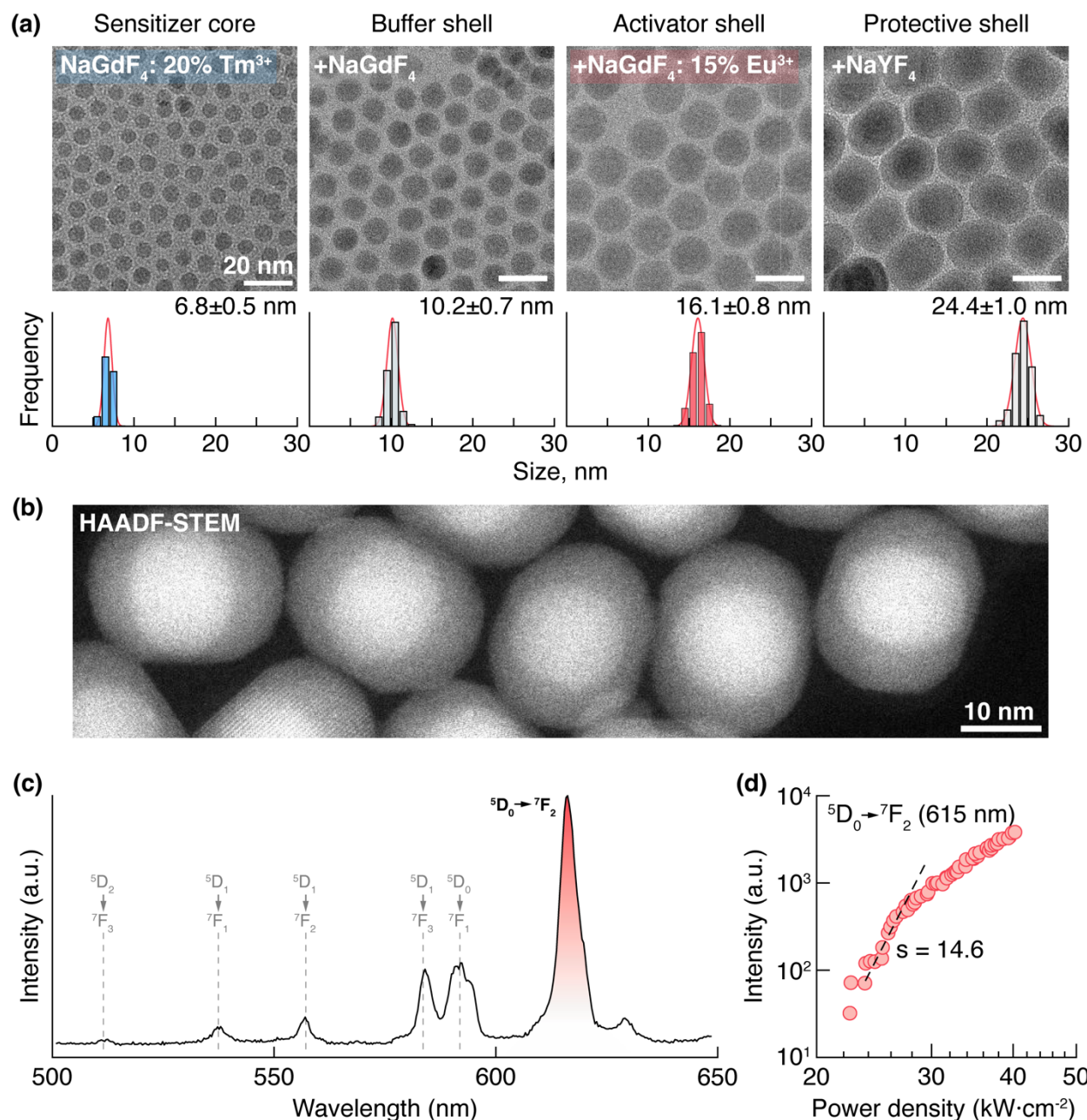


Figure 2. (a) Representative TEM micrographs of NaGdF₄: 20% Tm³⁺/NaGdF₄/NaGdF₄: 15% Eu³⁺/NaYF₄ ANPs following each synthesis step. Scale bar = 20 nm. Corresponding nanoparticle size distribution histograms together with average size and one standard size deviation are shown below each micrograph. (b) High-angle angular dark-field scanning transmission electron microscopy (HAADF-STEM) image of Eu³⁺-activated ANPs. (c) Eu³⁺ upconversion emission spectra in ANPs under 1064 nm excitation (49 kW·cm⁻²). The identified Eu³⁺ transitions are labeled next to each band. (d) Pump power dependence of Eu³⁺ [⁵D₀ → ⁷F₂; red-highlighted in (c)] emission

under 1064 nm excitation. Steepest intensity scaling with nonlinearity factor $s = 14.6$ is derived from linear fit of the log-log plot.

After establishing that EMU in ANPs can generate Eu^{3+} emission with high nonlinearity, we sought to corroborate the importance of energy migration within the Gd^{3+} network. To probe energy relay from the sensitizing Tm^{3+} core to the Eu^{3+} activator shell, we prepared a series of core/multishell NaGdF_4 : 20 mol% $\text{Tm}^{3+}/\text{NaY}_{1-x}\text{Gd}_x\text{F}_4/\text{NaGdF}_4$: 15 mol% $\text{Eu}^{3+}/\text{NaYF}_4$ ANPs in which the amount of Gd^{3+} in the intermediate buffer shell was varied ($x = 0.0, 0.2, 0.4, 1.0$) (**Supporting Information S4**). When no Gd^{3+} was present in the buffer shell ($x = 0$), energy transfer was suppressed and Tm^{3+} visible upconversion dominated the spectrum (**Figure 3a**, gray spectrum). When we introduced Gd^{3+} ions into the buffer shell ($x = 0.2-1.0$) Eu^{3+} upconversion (at 510 nm: $^5\text{D}_2 \rightarrow ^7\text{F}_3$) could be observed. The intensity of this Eu^{3+} emission line increased relative to that of Tm^{3+} (at 450 nm: $^1\text{D}_2 \rightarrow ^3\text{F}_4$) with increasing Gd^{3+} concentration, with the maximum Eu^{3+} emission intensity observed for the case of a NaGdF_4 buffer (**Figure 3a**, red spectrum). We were also able to measure steeply nonlinear Eu^{3+} emission in NaGdF_4 : 20 mol% $\text{Tm}^{3+}/\text{NaGdF}_4$: 15 mol% $\text{Eu}^{3+}/\text{NaYF}_4$ ANPs without the intermediate buffer shell (**Supporting Information S5**); however, two orders of magnitude greater laser power was required (grey data points in **Figure 3b**). The above observations reinforce the importance of the NaGdF_4 buffer shell for preventing direct Tm^{3+} - Eu^{3+} energy cross-talk while preserving EMU. As a further benefit, the buffer shell provides additional passivation of Tm^{3+} core from surface quenching.^[20,21]

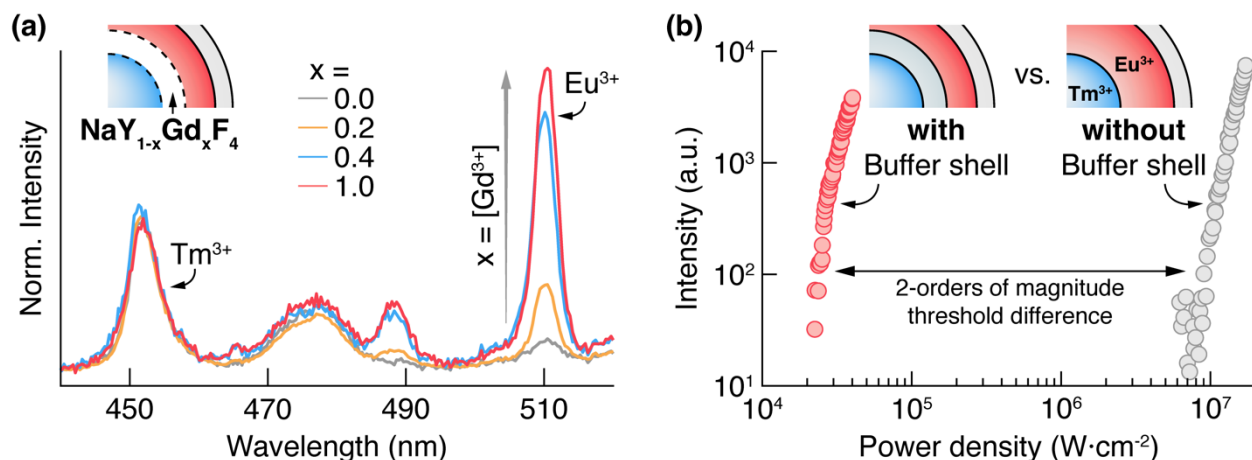


Figure 3. (a) Normalized upconversion of Eu^{3+} -activated ANPs with varying amounts of Gd^{3+} in the $\text{NaY}_{1-x}\text{Gd}_x\text{F}_4$ buffer shell ($x = 0.0, 0.2, 0.4, 1.0$). Spectra were acquired with $190 \text{ kW}\cdot\text{cm}^{-2}$ laser excitation power density to accentuate visible Tm^{3+} upconversion. (b) Pump power dependence of Eu^{3+} upconversion under 1064 nm excitation in ANPs with (red circles) and without (grey

circles) NaGdF₄ buffer shell. Two orders of magnitude greater pump powers are required to promote nonlinear Eu³⁺ emission in ANPs without the buffer shell.

Following the demonstration of remote PA in Eu³⁺-activated ANPs, we sought to extend this strategy to other A³⁺ ions to provide a generalized approach for spectral tuning of PA. We prepared a library of ANPs with Tm³⁺-doped cores and activator shells doped with either Tb³⁺, Er³⁺, Ho³⁺, Nd³⁺ or Dy³⁺ ions. These core/multishell ANPs share the same NaGdF₄:Tm³⁺ sensitizer core, NaGdF₄ intermediate buffer shell, and NaYF₄ outer protective shell (as in the Eu³⁺-activated ANPs shown in Figure 1a) – only the composition of the activator (NaGdF₄:A³⁺) shell is changed. The above ANPs were observed to have pure β -phase and diameters smaller than 25 nm (**Supporting Information S6**). Under 1064 nm excitation, each composition of ANPs featured a unique spectral profile of the selected A³⁺ activator in the visible spectrum (**Figure 4a, Figure S25**). We note that due to low upconversion intensity and unforeseen contamination by Er³⁺ ions, Nd³⁺ and Dy³⁺-activated ANPs were omitted from further studies. To validate that upconversion in spectrally discrete ANPs stems from PA and EMU, we irradiated Tm³⁺-free NaGdF₄: 2 mol% Er³⁺/NaYF₄ control nanoparticles with 1064 nm laser (**Supporting Information S7**). Er³⁺ upconversion was only detected at laser power densities greater than 1 MW·cm⁻², and its power dependence ($s = 1.8$) followed a two-photon process (**Figure S28b**). In contrast, emissions of different A³⁺ ions in spectrally discrete ANPs were generated in a highly nonlinear fashion, with nonlinearity factors s of 17.2, 11.1, and 10.7 observed for Tb³⁺, Ho³⁺, and Er³⁺-activated ANPs, respectively (**Figure 4b**).

Notably, power densities as low as 6 and 8 kW·cm⁻² were enough to promote visible PA upconversion from Er³⁺ and Ho³⁺-activated ANPs, respectively, similar to those originally reported for NaYF₄:Tm³⁺/NaYF₄:Gd³⁺ ANPs^[2] and substantially lower than other ANPs.^[5] In generating A³⁺ emission across spectrally discrete ANPs we observed some variation of the excitation power density threshold, being the lowest for Er³⁺-activated ANPs and the highest for Tb³⁺-activated ANPs (> 120 kW·cm⁻², **Figure 4b**). Although the spectrally discrete ANPs were prepared from the same batch of Tm³⁺-doped cores, we found no correlation between Tm³⁺ PA emission (800 nm) power thresholds (**Figure S29**) and that of respective A³⁺ ions; thus, the threshold variability cannot be attributed directly to the sensitizing core. We speculate that these discrepancies arise from small fluctuations in the thicknesses and growth inhomogeneities of buffer NaGdF₄ and protective NaYF₄ shells. The PA power threshold increases when energy can be directly passed between Tm³⁺ and A³⁺ ions (**Figure 3b**), as well as being highly sensitive to surface quenchers.^[21] Additionally, powers above 100 kW·cm⁻² can lead to photodarkening of Tm³⁺-based ANPs,^[8] which

further complicates measurements of PA emission from Tb³⁺-activated ANPs. Notwithstanding the power threshold differences, we can generalize that EMU spectral tuning can be adopted in ANPs for generating highly nonlinear emission ($s > 10$) from virtually any activator ion by the Tm³⁺ → Gd³⁺ → A³⁺ energy transfer cascade (**Figure 1b**, mechanism of Tm³⁺ excitation to ¹I₆ was informed by numerical simulations – see **Supporting Information S9** for details).

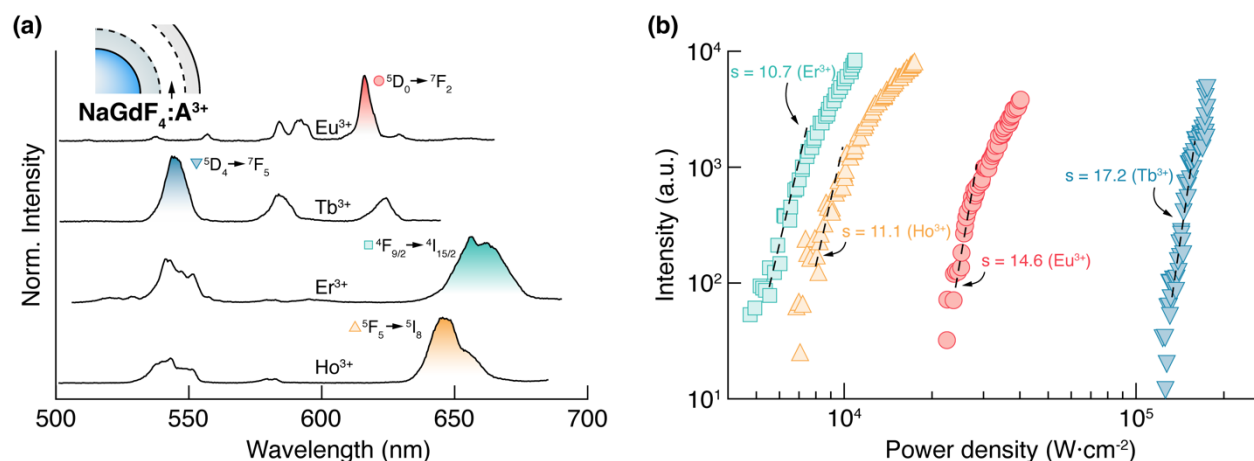


Figure 4. (a) Upconversion emission spectra in the 500-700 nm range of spectrally discrete ANPs containing different A³⁺ ions (Eu³⁺, Tb³⁺, Er³⁺ or Ho³⁺) in the activator shell under 1064 nm excitation. Spectra of Eu³⁺, Er³⁺, and Ho³⁺-activated ANPs were taken at 49 kW·cm⁻² laser power density, that of Tb³⁺-activated ANPs at 580 kW·cm⁻². (b) Pump power dependence of A³⁺ emission [shaded bands in (a)] intensities under 1064 nm excitation. Intensity scaling with nonlinearity factors $s = 10$ -17 is derived from linear fit of the log-log plot.

Inspired by the above results, we sought to demonstrate how EMU can facilitate the transfer of PA to external fluorophores. To demonstrate this concept, we optically characterized core/shell NaGdF₄: 20 mol% Tm³⁺/NaGdF₄ ANPs and core/multishell CdS/CdSe/CdS quantum dots (QDs) co-deposited on a glass coverslip (see **Supplementary Information S10** for details).^[22] Under 1064 nm excitation, photoluminescence of both ANPs and QDs could be directly observed (**Figure 5a**). ANP emission stemmed primarily from the ³H₄ → ³H₆ transition of Tm³⁺ ions at 800 nm, and a weaker band at 690 nm (³F_{2,3} → ³H₆) could be observed at high excitation powers. Importantly, this Tm³⁺ emission had minimal overlap with the QD emission observed at 630 nm (**Figure S35b**). Although the QDs alone could be excited with 1064 nm laser via two-photon excitation (TPE; **Figure S35c**), in the presence of ANPs their emission intensity increased beyond the quadratic scaling observed without ANPs (**Figure S36a**). The excitation of QDs by ANP → QD energy transfer resulted in QD emission power dependence with $s = 10.5$ (purple data points

in **Figure 5b**; background signal of QD photoluminescence by direct 1064 nm excitation was subtracted from raw data prior to log-log plot fitting). The PA emission of ANPs (blue data points in **Figure 5b**) in the ANP+QD avalanching complex had lower power threshold and higher degree of nonlinearity ($s = 15.8$), as expected since energy transfer to QDs requires ANP excitation into high energy states and introduces additional relaxation pathways. These experiments corroborate the involvement of $\text{Tm}^{3+} \rightarrow \text{Gd}^{3+} \rightarrow \text{QDs}$ energy transfer cascade at around $70 \text{ kW}\cdot\text{cm}^{-2}$ (for the present combination of nanoparticles).

To further justify QD activation by $\text{Gd}^{3+} \rightarrow \text{QDs}$ energy transfer, we tested $\text{NaGdF}_4: 20\% \text{ Tm}^{3+}/\text{NaYF}_4$ ANPs as energy donors for QDs, in which case the energy transfer from ANPs to QDs was expected to be minimized by the undoped NaYF_4 shell. We observed a slight deviation from the quadratic TPE power-scaling of QD emission in the mixture with $\text{NaGdF}_4:\text{Tm}^{3+}/\text{NaYF}_4$ ANPs above $100 \text{ kW}\cdot\text{cm}^{-2}$, however the degree of nonlinearity was significantly lower ($s = 6.7$, **Figure S36b**). Since both ANPs (with NaGdF_4 or NaYF_4 outer shell) show near identical Tm^{3+} -PA (measured by 800 nm emission), we hypothesize that radiative energy-transfer from $\text{NaGdF}_4:\text{Tm}^{3+}/\text{NaYF}_4$ ANPs to QDs at high excitation powers can still promote a more nonlinear QD photoluminescence. Altogether, we successfully extended PA from ANPs to other fluorophores via interparticle EMU, demonstrating the ability to form avalanching complexes for highly sensitive multiplexing and sub-diffraction imaging assays.^[23,24]

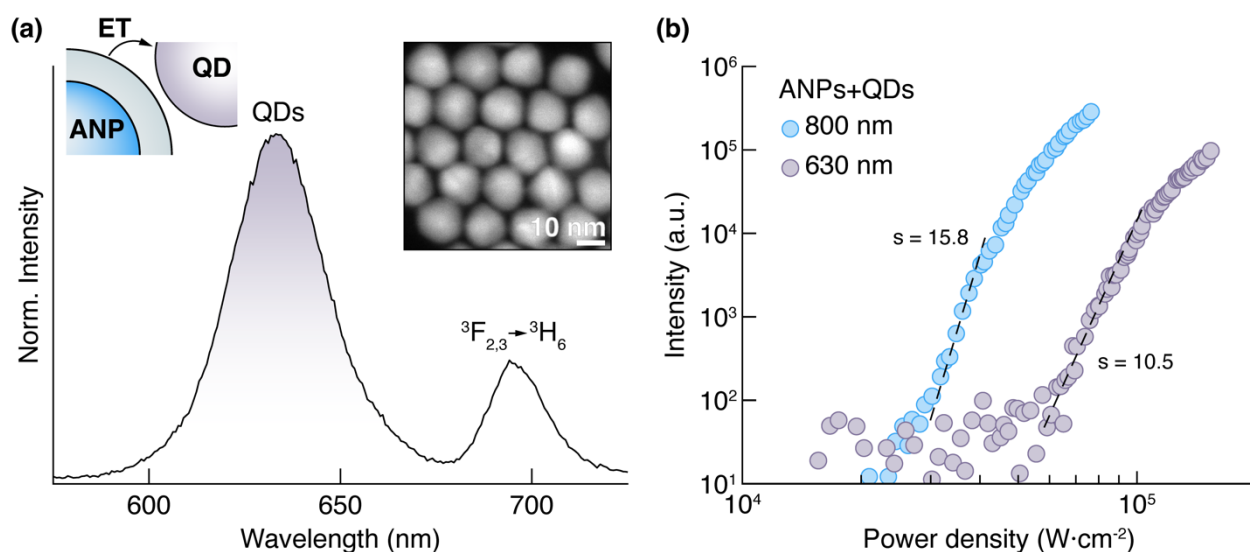


Figure 5. (a) Upconversion emission spectra of co-deposited $\text{NaGdF}_4:\text{Tm}^{3+}/\text{NaGdF}_4$ ANPs and CdS/CdSe/CdS QDs under 1064 nm excitation ($100 \text{ kW}\cdot\text{cm}^{-2}$). ET – energy transfer. Inset: HAADF-STEM image of QDs; scale bar = 10 nm. (b) Pump power dependence of ANP (Tm^{3+} at 800 nm; blue data points) and QD (630 nm as highlighted in (a); purple data points) emission

intensities under 1064 nm excitation. The steepest intensity scaling and corresponding nonlinearity factors (shown in the figure) are derived from a linear fit of the log-log plot.

In summary, we demonstrate that the combination of Tm³⁺-based PA and Gd³⁺-assisted EMU is an effective approach to tune the emission spectra of photon avalanching nanoparticles. Using spectrally discrete ANPs, upconversion profiles of Er³⁺, Ho³⁺, Eu³⁺, Nd³⁺, Dy³⁺, and Tb³⁺ were observed under 1064 nm excitation, with highly nonlinear intensity power-scaling ($s = 10-17$). Through rational design of the heterostructured ANPs, PA emission of activators was generated in nanocrystals as small as 25 nm in diameter and at exceptionally low laser excitation power densities ($<10 \text{ kW}\cdot\text{cm}^{-2}$). Importantly, we found that PA can be extended beyond lanthanide ions, as demonstrated by PA-like emission of semiconductor QDs in ANP+QD avalanching complexes – which showcases how extreme nonlinearities can be imprinted onto linear emitters. We believe that these findings represent a significant step forward in developing ANPs with customizable compositions, tunable photoluminescence properties, and synergistic interaction with other fluorophores – with potential application in multicolor sub-diffraction imaging, surface patterning, and ultra-sensitive bioassays.

Methods

Detailed information regarding the nanoparticle synthesis, structural and spectroscopic characterization is provided in the Supporting Information.

Associated content

Supporting Information. Complete ANP and QD synthesis and characterization description. Additional XRD, TEM and photoluminescence data; including Scheme 1, Figures S1-S36, Tables S1-S4 (PDF).

Notes

The authors declare no competing financial interest.

Acknowledgements

A.S. acknowledges support from the European Union's Horizon 2020 research and innovation program under the Marie Skłodowska-Curie Grant Agreement No. 895809 (MONOCLE). Work at the Molecular Foundry was supported by the U.S. Department of Energy (DOE) under Contract

No. DE-AC02-05CH11231 through the Office of Science, Office of Basic Energy Sciences and J. A. through the Chemical Sciences, Geosciences, and Biosciences Division, Separations Program. H.Y. and quantum dot synthesis were supported by the DOE Office of Energy Efficiency and Renewable Energy (EERE), under Award Number DE-EE0007628. X.Q., B.E.C., and E.M.C. were supported by the Defense Advanced Research Projects Agency (DARPA) under Contract No. HR0011257070. C.L and P.J.S. acknowledge support from DARPA Contract No. HR00112220006 and from the National Science Foundation grant CHE-2203510. This work was financed by the Spanish Ministerio de Innovación y Ciencias under Project No. NANONERV PID2019- 106211RB-I00 and by the Comunidad Autónoma de Madrid (S2022/BMD-7403 RENIM-CM).

References

- (1) Joubert, M.-F. Photon Avalanche Upconversion in Rare Earth Laser Materials. *Opt. Mater.* **1999**, *11* (2–3), 181–203.
- (2) Lee, C.; Xu, E. Z.; Liu, Y.; Teitelboim, A.; Yao, K.; Fernandez-Bravo, A.; Kotulska, A. M.; Nam, S. H.; Suh, Y. D.; Bednarkiewicz, A.; Cohen, B. E.; Chan, E. M.; Schuck, P. J. Giant Nonlinear Optical Responses from Photon-Avalanching Nanoparticles. *Nature* **2021**, *589* (7841), 230–235.
- (3) Dudek, M.; Szalkowski, M.; Misiak, M.; Cwierzona, M.; Skripka, A.; Korczak, Z.; Piątkowski, D.; Woźniak, P.; Lisiecki, R.; Goldner, P.; Maćkowski, S.; Chan, E. M.; Schuck, P. J.; Bednarkiewicz, A. Size-Dependent Photon Avalanching in Tm³⁺ Doped LiYF₄ Nano, Micro, and Bulk Crystals. *Adv. Opt. Mater.* **2022**, 2201052.
- (4) Zhang, Z.; Skripka, A.; Dahl, J. C.; Dun, C.; Urban, J. J.; Jaque, D.; Schuck, P. J.; Cohen, B. E.; Chan, E. M. Tuning Phonon Energies in Lanthanide-doped Potassium Lead Halide Nanocrystals for Enhanced Nonlinearity and Upconversion. *Angew. Chem. Int. Ed.* **2023**, *62* (1), e202212549.
- (5) Liang, Y.; Zhu, Z.; Qiao, S.; Guo, X.; Pu, R.; Tang, H.; Liu, H.; Dong, H.; Peng, T.; Sun, L.-D.; Widengren, J.; Zhan, Q. Migrating Photon Avalanche in Different Emitters at the Nanoscale Enables 46th-Order Optical Nonlinearity. *Nat. Nanotechnol.* **2022**, *17* (5), 524–530.
- (6) Denkova, D.; Ploschner, M.; Das, M.; Parker, L. M.; Zheng, X.; Lu, Y.; Orth, A.; Packer, N. H.; Piper, J. A. 3D Sub-Diffraction Imaging in a Conventional Confocal Configuration by Exploiting Super-Linear Emitters. *Nat. Commun.* **2019**, *10* (1), 3695.
- (7) Bednarkiewicz, A.; Chan, E. M.; Kotulska, A.; Marciniak, L.; Prorok, K. Photon Avalanche in Lanthanide Doped Nanoparticles for Biomedical Applications: Super-Resolution Imaging. *Nanoscale Horiz.* **2019**, *4* (4), 881–889.
- (8) Lee, C.; Xu, E. Z.; Kwock, K. W. C.; Teitelboim, A.; Liu, Y.; Fardian-Melamed, N.; Pedroso, C. C. S.; Park, H. S.; Kim, J.; Pritzl, S. D.; Nam, S. H.; Lohmueller, T.; Ercius, P.; Suh, Y. D.; Cohen, B. E.; Chan, E. M.; Schuck, P. J. Indefinite and Bidirectional Near Infrared Nanocrystal Photoswitching, 2022.
- (9) Bednarkiewicz, A.; Chan, E. M.; Prorok, K. Enhancing FRET Biosensing beyond 10 Nm with Photon Avalanche Nanoparticles. *Nanoscale Adv.* **2020**, *2* (10), 4863–4872.
- (10) Szalkowski, M.; Dudek, M.; Korczak, Z.; Lee, C.; Marciniak, Ł.; Chan, E. M.; Schuck, P. J.; Bednarkiewicz, A. Predicting the Impact of Temperature Dependent Multi-Phonon Relaxation Processes on the Photon Avalanche Behavior in Tm³⁺: NaYF₄ Nanoparticles. *Opt. Mater.: X* **2021**, *12*, 100102.
- (11) Wang, F.; Deng, R.; Wang, J.; Wang, Q.; Han, Y.; Zhu, H.; Chen, X.; Liu, X. Tuning Upconversion through Energy Migration in Core–Shell Nanoparticles. *Nat. Mater.* **2011**, *10* (12), 968–973.
- (12) Xu, E. Z.; Lee, C.; Pritzl, S. D.; Chen, A. S.; Lohmueller, T.; Cohen, B. E.; Chan, E. M.; Schuck, P. J. Infrared-to-Ultraviolet Upconverting Nanoparticles for COVID-19-Related Disinfection Applications. *Opt. Mater.: X* **2021**, *12*, 100099.
- (13) Levy, E. S.; Tajon, C. A.; Bischof, T. S.; lafrati, J.; Fernandez-Bravo, A.; Garfield, D. J.; Chamanzar, M.; Maharbiz, M. M.; Sohal, V. S.; Schuck, P. J.; Cohen, B. E.; Chan, E. M. Energy-Looping Nanoparticles: Harnessing Excited-State Absorption for Deep-Tissue Imaging. *ACS Nano* **2016**, *10* (9), 8423–8433.
- (14) Chan, E. M.; Xu, C.; Mao, A. W.; Han, G.; Owen, J. S.; Cohen, B. E.; Milliron, D. J. Reproducible, High-Throughput Synthesis of Colloidal Nanocrystals for Optimization in Multidimensional Parameter Space. *Nano Lett.* **2010**, *10* (5), 1874–1885.
- (15) Wang, X.; Yan, L.; Liu, S.; Zhang, P.; Huang, R.; Zhou, B. Enhancing Energy Migration Upconversion through a Migratory Interlayer in the Core–Shell–Shell Nanostructure towards Latent Fingerprinting. *Nanoscale* **2020**, *12* (36), 18807–18814.

- (16) Su, Q.; Han, S.; Xie, X.; Zhu, H.; Chen, H.; Chen, C.-K.; Liu, R.-S.; Chen, X.; Wang, F.; Liu, X. The Effect of Surface Coating on Energy Migration-Mediated Upconversion. *J. Am. Chem. Soc.* **2012**, *134* (51), 20849–20857.
- (17) Pedroso, C. C. S.; Mann, V. R.; Zuberbühler, K.; Bohn, M.-F.; Yu, J.; Altoe, V.; Craik, C. S.; Cohen, B. E. Immunotargeting of Nanocrystals by SpyCatcher Conjugation of Engineered Antibodies. *ACS Nano* **2021**, *15* (11), 18374–18384.
- (18) Voronovic, E.; Skripka, A.; Jarockyte, G.; Ger, M.; Kuciauskas, D.; Kaupinis, A.; Valius, M.; Rotomskis, R.; Vetrone, F.; Karabanovas, V. Uptake of Upconverting Nanoparticles by Breast Cancer Cells: Surface Coating versus the Protein Corona. *ACS Appl. Mater. Interfaces* **2021**, *13* (33), 39076–39087.
- (19) Pan, J.-A.; Wu, H.; Gomez, A.; Ondry, J. C.; Portner, J.; Cho, W.; Hinkle, A.; Wang, D.; Talapin, D. V. Ligand-Free Direct Optical Lithography of Bare Colloidal Nanocrystals via Photo-Oxidation of Surface Ions with Porosity Control. *ACS Nano* **2022**, *16* (10), 16067–16076.
- (20) Fischer, S.; Bronstein, N. D.; Swabeck, J. K.; Chan, E. M.; Alivisatos, A. P. Precise Tuning of Surface Quenching for Luminescence Enhancement in Core–Shell Lanthanide-Doped Nanocrystals. *Nano Lett.* **2016**, *16* (11), 7241–7247.
- (21) Kwock, K. W. C.; Lee, C.; Teitelboim, A.; Liu, Y.; Yao, K.; Alam, S. B.; Cohen, B. E.; Chan, E. M.; Schuck, P. J. Surface-Sensitive Photon Avalanche Behavior Revealed by Single-Avalanching-Nanoparticle Imaging. *J. Phys. Chem. C* **2021**, *125* (43), 23976–23982.
- (22) Marin, R.; Labrador-Paéz, L.; Skripka, A.; Haro-González, P.; Benayas, A.; Canton, P.; Jaque, D.; Vetrone, F. Upconverting Nanoparticle to Quantum Dot Förster Resonance Energy Transfer: Increasing the Efficiency through Donor Design. *ACS Photonics* **2018**, *5* (6), 2261–2270.
- (23) Pini, F.; Francés-Soriano, L.; Andrigo, V.; Natile, M. M.; Hildebrandt, N. Optimizing Upconversion Nanoparticles for FRET Biosensing. *ACS Nano* **2023**, *17* (5), 4971–4984.
- (24) Kotulska, A. M.; Pilch-Wróbel, A.; Lahtinen, S.; Soukka, T.; Bednarkiewicz, A. Upconversion FRET Quantitation: The Role of Donor Photoexcitation Mode and Compositional Architecture on the Decay and Intensity Based Responses. *Light Sci. Appl.* **2022**, *11* (1), 256.